

XMM-Newton observations of H₂O maser galaxy NGC 7479 *

Jin Wang, Jiang-Shui Zhang and Jun-Hui Fan

Center for Astrophysics, Guangzhou University, Guangzhou 510006, China; jszhang@gzhu.edu.cn

Received 2009 June 17; accepted 2010 May 24

Abstract The XMM-Newton observations of H₂O megamaser galaxy NGC 7479 are presented. Its smoothed X-ray image clearly shows spiral morphology, which matches well with its optical asymmetric spiral structure. One prominent source can be found at the tip of its northern spiral arm, which is much brighter than its nuclear X-ray source (about a 50% higher count rate). For the nuclear source (a circular region with a radius of 20''), the spectra show soft excess below 2 keV and a strong iron K α emission line. The best fitting model includes a partially absorbed model for the hard continuum and one thermal plasma model for the soft scatter component. Both the high column density ($N_{\text{H}} \sim 6.88 \times 10^{23} \text{ cm}^{-2}$) and strong fluorescent iron line (with an equivalent width of $\sim 1.5 \text{ keV}$) support the existence of one heavily obscured AGN. For the bright prominent source, its radial profile is consistent with that of a single point-like source. Its spectra are extracted from the circular region around its peak, with a radius of 20'' and 6'' respectively and both spectra show no significant difference. Four alternative models for the ultra-luminous X-ray source (ULXs) can reproduce the spectra well: an absorbed power law, thermal bremsstrahlung, multicolor blackbody disk plus another blackbody or power law. Further observations (e.g., the tremendous improvement in the spatial resolution of the Chandra X-ray observations) and studies are desirable for probing the nature of this prominent source. In addition, we also estimate the mass of its central engine to be $1.18 \times 10^7 M_{\odot}$ and maser disk parameters: the disk radius of $\sim 0.7 \text{ pc}$ and the dimensionless accretion rate ($L_{2-10\text{keV}}/L_{\text{Edd}}$) of 1.2×10^{-4} .

Key words: masers — galaxies: active — galaxies: nuclei — galaxies: individual (NGC 7479) — X-rays: galaxies

1 INTRODUCTION

Because of its ultraluminosity, an H₂O megamaser ($L > L_{\odot}$) has been considered to be related to an AGN, which is supported by statistical analysis of maser luminosity, nuclear X-ray luminosity, and central black hole mass (Kondratko et al. 2006; Su et al. 2008). It has become one of the best targets for high resolution imaging to probe the innermost region of the maser's host AGN and further determine high-accuracy geometric distances, estimate the Hubble constant independently of the systematic uncertainties and constrain the fundamental nature of dark energy (e.g., Braatz 2009). Observations show that H₂O maser spots are located preferentially in the obscured nuclear

* Supported by the National Natural Science Foundation of China.

regions of Seyfert 2 or LINERs and most of them are heavily obscured ($N_{\text{H}} > 10^{23} \text{ cm}^{-2}$), and are even Compton-thick ($N_{\text{H}} > 10^{24} \text{ cm}^{-2}$; Braatz et al. 1997; Madejski et al. 2006; Zhang et al. 2006; Greenhill et al. 2008; Zhang et al. 2010). For X-ray penetrability, observations of nuclear hard X-ray emission provide one effective method to probe those obscured nuclear regions with maser spots.

The barred galaxy NGC 7479 has been detected with H_2O maser emission in its nuclear region (Braatz & Gugliucci 2008). Its nucleus is classified as a starburst (Devereux 1989), or a LINER (Low Ionizing Nuclear Emission Region, Keel 1983) and a type 1.9 Seyfert galaxy (Ho et al. 1997). Its optical image shows a strongly barred and asymmetric spiral structure, strong and long western spiral arms and a poorly organized eastern spiral (Quillen et al. 1995). Since the galaxy is isolated (Tully 1988), a very recent or even on-going minor-merger is suggested to explain the strong bars and asymmetric spiral structure (Quillen et al. 1995; Laine & Heller 1999). The minor merger models predict that the nuclear remnant of a mostly disrupted companion should currently be in the bar, north of the nucleus, coinciding with the perturbation in the $\text{H}\alpha$ velocity field (Laine & Heller 1999). Its VLA radio continuum shows the existence of a bright, broader and less polarized jet almost in the plane of the host galaxy (Laine & Beck 2008). Sensitive X-ray observations should be useful to clearly show the interaction between the large jet and the dense interstellar medium in the disk.

From the High Energy Astrophysics Science Archive Research Center (HEASARC), the source was observed by the X-ray satellite ASCA (low sensitivity) and *XMM-Newton*, and there is no published paper as yet. Here observational data from the highly sensitive *XMM-Newton* archive data are used to analyze its detailed X-ray emission morphology and probe its obscured maser environment.

Throughout the paper, we adopt a Galactic absorption column density of $N_{\text{H}} \sim 5.29 \times 10^{20} \text{ cm}^{-2}$ (LAB survey, see Kalberla et al. 2005). The distance is $D \sim 31.7 \text{ Mpc}$, where $1''$ corresponds to $\sim 152 \text{ pc}$ (From Cosmology Calculators I in the NASA/IPAC Extragalactic Database (NED), assuming a Hubble law with $H_0 = 75 \text{ km s}^{-1} \text{ Mpc}^{-1}$, $\Omega_M = 0.270$, $\Omega_{\text{vac}} = 0.730$ and a redshift of 0.007942).

2 DATA ACQUISITION AND REDUCTION

XMM-Newton observed NGC 7479 on 2001 June 19¹ with an exposure time of 13 ks and on 2005 June 24² with an exposure time of 16 ks. The second observation suffered heavily from background flares. Thus, we only use the data obtained from the first observation in our paper.

The European Photon Imaging Camera (EPIC) with MOS (mos 1 and mos 2) and PN detectors of the first observation was utilized in the full frame mode with the medium filter. The archived data are downloaded from the *XMM-Newton* Science Archive (XSA) and processed with the SAS v8.0 package and the latest available calibration constituent files. We use the SAS standard pipeline processing meta tasks ‘*emproc*’ and ‘*epproc*’ for processing the raw MOS and PN data files to generate the relative calibrated event lists. Then the event lists are filtered to exclude bad events and periods of high background, using the SAS task ‘*evselect*’ with the $\text{PATTERN} \leq 12$ and XMMEA_EM for MOS and the $\text{PATTERN} \leq 4$ and XMMEA_EP for PN. To identify intervals with flaring particle background, we extract the high energy light curve in the $> 10 \text{ keV}$ (MOS) and the 10-12 keV band (PN) and determine a threshold for the light curve counts ($0.20 \text{ counts s}^{-1}$ for MOS and $0.25 \text{ counts s}^{-1}$ for PN). Then, we create a corresponding GTI file by running the task ‘*tabgtigen*’ and use it to filter the calibrated event list. After excluding the contaminated intervals, we obtain the net exposure time $\sim 8.3 \text{ ks}$ (MOS) and $\sim 5.8 \text{ ks}$ (PN) for the next part of the analysis. Only the events with ‘FLAG=0’ are selected for spectral analysis.

¹ Obs.ID: 0025541001; PI: Kazushi Iwasawa

² Obs.ID: 0301651201; PI: Ioannis Georgantopoulos

3 DATA ANALYSIS

3.1 Spatial Analysis

One faint nucleus (99 counts for the nine brightest pixels around the center in the binned image with a bin size of 80) can be found in the filtered raw image in the 0.15–15 keV band. One strikingly bright source can be found at the tip of its northern arm (392 counts for the nine brightest pixels around the center in the binned image with a bin size of 80), $\sim 80''$ away from the nucleus (2XMM J230457.6+122028, from the *XMM-Newton* Science Archive Center). However, no significant counterparts can be found in other wave-bands, such as the $H\alpha$ image, radio or infrared images. Another prominent feature is one fuzzy spiral arm shape around the faint nucleus. To clearly show the X-ray spiral structure, an adaptively smoothed three-color image of NGC 7479 in the band 0.3–8.0 keV is created by using the *XMM-Newton* image script from the SAS analysis thread (the image script, a package for creating attractive *XMM-Newton* images). The smoothed image clearly shows spiral morphology, especially in the western arm, which agrees well with the optical asymmetric spiral structure (as does its ultraviolet image, from GALEX, the Galaxy Evolution Explorer). For the faint nucleus, its emission morphology shows south-north extension, which seems to match the orientation of its jet (Laine & Beck 2008). X-ray observations with high resolution are needed to explore the association of the extended nuclear X-ray emission and the jet. The X-ray peak ($23^{\text{h}}04^{\text{m}}56.37^{\text{s}}$, $+12^{\circ}19'21.77''$, with a positional accuracy of $\sim 1.28''$ from the http://xmm2.esac.esa.int/external/xmm_data_acc/xsa/browser/xsa.html) agrees well with that of its optical image ($23^{\text{h}}04^{\text{m}}56^{\text{s}}.69$, $+12^{\circ}19'23''.2$, with an uncertainty of $1.7''$ from the NED). For comparison, Figure 1 presents both the smoothed X-ray image (left panel) and its DSS (Digitized Sky Survey) optical image with overlaid X-ray intensity contours (right panel).

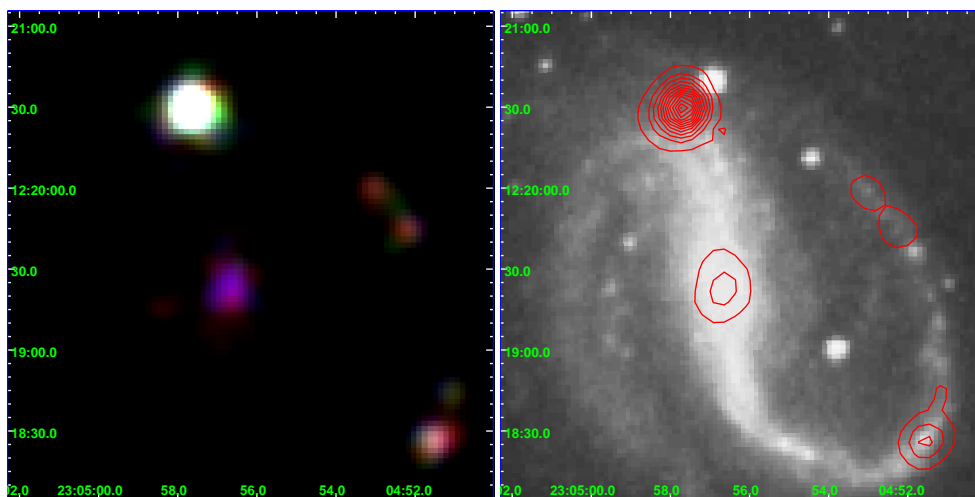


Fig. 1 *Left panel:* Adaptively smoothed three-color *XMM-Newton* image of NGC 7479 in 0.3–8.0 keV (on a linear scale). Red represents soft emission between 0.3 keV and 1.5 keV, green corresponds to 1.5 keV to 2.5 keV and blue for 2.5 keV to 8.0 keV. *Right panel:* its optical image on a linear scale from the DSS (Digitized Sky Survey), overlaid by the EPIC 0.3–8 keV intensity contours. The lowest contour is $4 \text{ counts pixel}^{-1}$, with an increment of $4 \text{ counts pixel}^{-1}$.

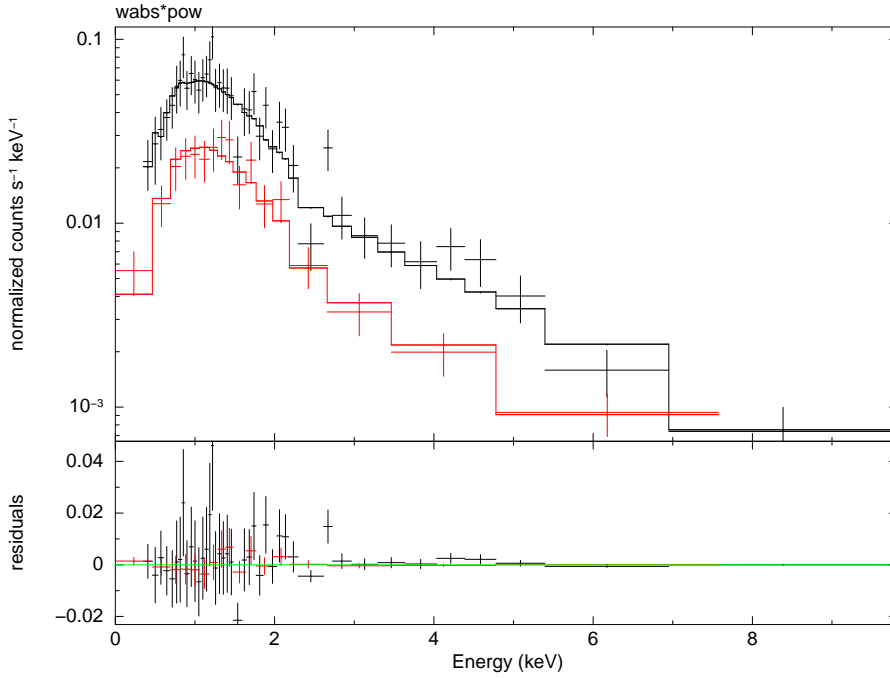


Fig. 2 Spectra of the prominent bright source 2XMM J230457.6+122028 from circles with a radius of 20'' (black) and 6'' (red) around the peak position (see electronic version). A single power law model (histograms) can fit both spectra well. Residuals are shown in the lower panel.

In order to check the possible variability, we extract X-ray lightcurves with various time intervals for both the nuclear source and the brightest source (2XMM J230457.6+122028) respectively and their background lightcurves are subtracted by using the SAS task ‘*epiclcorr*.’ No significant variability can be found in both lightcurves during the effective exposure time. The mean count rate is ~ 0.1 counts s^{-1} for the nuclear source and ~ 0.15 counts s^{-1} for the prominent source 2XMM J230457.6+122028.

In the following, we focus on spectral analysis for the nuclear source and the prominent source 2XMM J230457.6+122028. For these two sources, we extract the spectra from circles with a radius of 20'' using the aperture around the source position and background spectra from nearby regions free of other X-ray sources in the same CCD binned image (bin size of 80). The appropriate RMF (Redistribution Matrix File) and ARF (Ancillary Response File) of both sources are created using the SAS tasks ‘*rmfgen*’ and ‘*arfgen*.’ Spectra and response matrices of two MOS cameras are combined together by using the FTOOL task ‘*addspec*,’ to increase the signal-to-noise due to the low number of photon counts of mos 1 and mos 2. Then for the χ^2 statistics, spectra (MOS and PN) are grouped to contain 10 counts per bin for the fainter nuclear source and 20 counts per bin for the brightest source by using the ‘*grppha*’ task in the FTOOLS software.

For its extension, it is necessary to examine whether 2XMM J230457.6+122028 is consistent with a point-like source. First, the spectra are extracted from the smaller central region with a radius of $\sim 6''$ (the brightest four pixels in the binned image with a bin size of 80). Both its 6'' and 20'' spectra as well as their fitting curves by a single power law are presented in Figure 2. Although there may be some features around 2–5 keV (e.g., an emission line feature around ~ 2.7 keV in

the 20'' spectra), it is difficult to give a detailed analysis from the available spectra. Fitting results for both spectra are very consistent, including the spectral index, absorption column density and unabsorbed X-ray luminosity, etc. (see details in Table 1). This result suggests that the object under study is consistent with a point-like source. Furthermore, the radial profile with a size of 30'' of the prominent source is extracted by the SAS task '*eradial*' and fitted with the nominal point spread function (PSF) from a calibration file using 0.5 keV, 1 keV, 1.5 keV and 2 keV respectively. All radial profiles can be well fitted by the nominal point spread function, the King profile, which matches a point source (1.5 keV results shown in Fig. 3). So, we ascribe the X-ray emission from this region to be a single point-like source and the spectrum from 20'' is used in the following analysis, because of its relatively high counts. However, analysis of the coming Chandra data³ will ultimately be more helpful to more precisely determine its nature.

Table 1 Comparison of Fitting Results between 20'' and 6'' PN Spectra of the Brightest X-ray Source 2XMM J230457.6+122028

Radius ''	N_{H}^a (10^{22} cm^{-2})	Γ^b	$L_{2-10 \text{ keV}}^{\text{int}c}$ ($10^{40} \text{ erg s}^{-1}$)	$L_{0.5-10 \text{ keV}}^{\text{int}d}$ ($10^{40} \text{ erg s}^{-1}$)	$\chi^2/\text{d.o.f}$
20	0.26 ± 0.03	1.97 ± 0.11	4.5	8.2	45.46/53
6	0.30 ± 0.05	2.06 ± 0.19	1.9	3.6	45.46/53

A single power-law model was used to fit both spectra.

^a X-ray line-of-sight absorbing column density.

^b The photon index.

^{c,d} The 2–10 keV and 0.5–10 keV intrinsic luminosity respectively.

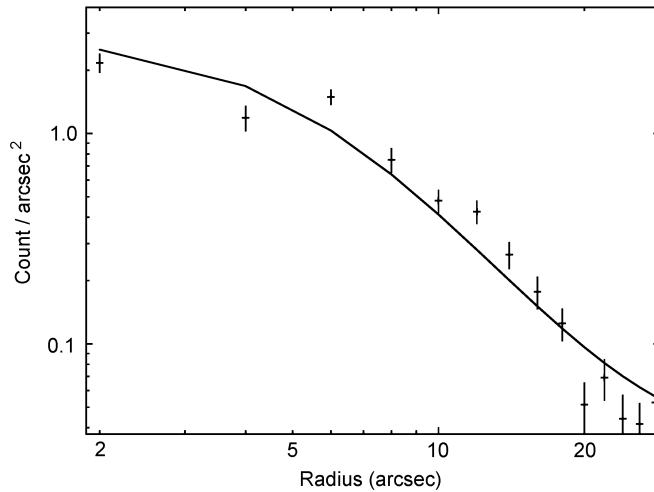


Fig. 3 Radial profile of the prominent source 2XMM J230457.6+122028 at 1.5 keV and the fitting curve from the nominal point spread function (King profile).

³ Obs.ID: 11230 (August 11, 2009) and 10120 (October 24, 2009); PI: David Pooley

3.2 Spectral Analysis

For both sources, spectral fits are performed simultaneously on spectra from both EPIC cameras MOS (mos 1+mos 2) and PN spectra, using the XSPEC v12.4.0 package. All errors quoted below correspond to the 90% confidence level for the interesting parameter, i.e., $\Delta\chi^2 = 2.71$.

3.2.1 Nuclear source

A simple power law model is first tried to fit the nuclear spectra. The fitting results are statistically totally unacceptable with $\chi^2=131.5/37$ d.o.f. (degrees of freedom). Residuals in terms of sigma show significant soft X-ray excess below 2 keV and one remarkable feature around 6.4 keV, which should be the iron $K\alpha$ fluorescent line.

Then the common model for Seyfert 2 spectra is applied, i.e., the two power law model (with the same photon index), which is an absorbed power law for the hard nuclear emission and another one for the scattering component of the hard component (e.g., Moran et al. 2001). For the remarkable residuals around 6.4 keV, the iron emission line is also included. The spectra can be reproduced with a photon index of $\Gamma = 2.41 \pm 0.14$, but the statistical χ^2 value shows a slightly large value (52.52/37, for model I in Table 2). Then two alternative physical models are considered to describe the hard nuclear X-ray emission: a Compton-thick high-energy reflection spectrum (model II, absorbing column density N_{H} in excess of 10^{24} cm^{-2}) and a partially absorbed power law spectrum (model III, N_{H} typically from 10^{22} cm^{-2} to a few times 10^{23} cm^{-2}) (e.g., Zhang et al. 2006). The soft component is modeled via a thermal MEKAL plasma model (e.g., Mewe et al. 1985). Although fitting results from both models are acceptable, the Compton-thick high-energy reflection model is statistically inferior to our preferred model (the partially absorbed power law model, with a reduced χ^2 value of ~ 0.7 for 26 degrees of freedom, see Fig. 4). Moreover, the former model implies an index with a relatively bigger error (2.37 ± 0.77), while the photon index from the later (2.08 ± 0.42) is consistent with the typical value of Seyfert 2 galaxies.

The detailed fitting results are listed in Table 2. They undoubtedly demonstrate the presence of the strong iron line (with equivalent width (EW) of ~ 1.5 keV from our preferred model III, see details in Table 2). Furthermore, high absorbing column density can also be found ($N_{\text{H}} > 10^{24} \text{ cm}^{-2}$ and $N_{\text{H}} \sim 6.9 \times 10^{23} \text{ cm}^{-2}$ from models II and III respectively). *Mekal* can fit the soft component well with a plasma temperature of ~ 0.55 keV. The observed 0.5–2.0 keV flux and 2.0–10.0 keV flux are $3.27 \times 10^{-14} \text{ erg cm}^{-2} \text{ s}^{-1}$ and $2.40 \times 10^{-13} \text{ erg cm}^{-2} \text{ s}^{-1}$ respectively.

Table 2 Spectral Fitting Results of the Nuclear Source

Model	N_{H}^a (10^{22} cm^{-2})	Γ^b	kT^c (keV)	E_{Fe}^d (keV)	σ_{Fe}^e (eV)	EW ^f (keV)	$\chi^2/\text{d.o.f}$
I	78.45 ± 20.65	2.41 ± 0.14	—	6.40 ± 0.03	70 ± 70	~ 1.2	50.52/37
II	> 100	2.37 ± 0.77	0.49 ± 0.08	6.39 ± 0.03	150 ± 40	~ 3.8	39.58/37
III	68.78 ± 18.67	2.08 ± 0.42	0.55 ± 0.10	6.40 ± 0.03	70 ± 60	~ 1.5	25.98/37

Model I: the two power law model (wabs*(pow+zwasb(pow+gau)) in XSPEC), Model II: a Compton-thick high-energy reflection model (wabs*(mekal+hrefl(pow+gau))), Model III (our preferred model): a partially absorbed power law model (wabs*(mekal+pow+zwasb(pow+gau))). The same photon index was set for the two-power-law model.

^a X-ray absorbing column density.

^b The photon index.

^c The temperature of the thermal plasma.

^{d,e,f} The centroid energy, the line width and the equivalent width of the iron $K\alpha$ line, respectively.

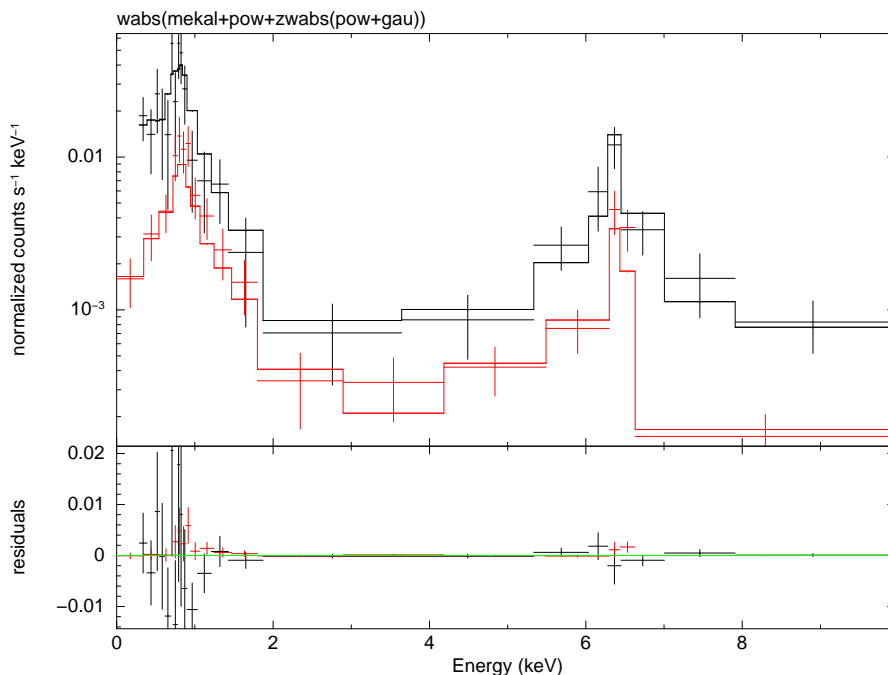


Fig. 4 Nuclear spectra and the best-fitting model (partially absorbed power law and thermal plasma emission, $wabs*(mekal+pow+zwabs(pow+gau))$). Crosses mark the observed fluxes and the histograms show the fitting model. Residuals are shown in the lower panel. *Black*: PN spectrum, *red*: MOS spectrum (see electronic version).

3.2.2 The brightest X-ray source 2XMM J230457.6+122028

Spectra from this source show few counts over 6 keV and no feature of the iron emission line can be found. For this type of bright source that is located in the spiral arm of the spiral galaxy, three general models are initially attempted: power law, thermal bremsstrahlung and multicolor blackbody disk (MCD) model (e.g., Makishima et al. 2000; Luo et al. 2007; Kajava & Poutanen 2009; Swartz et al. 2004; Reynolds et al. 1997). The absorption column density is set to be a free parameter. Both the power law and the thermal bremsstrahlung models can describe the data well (statistical χ^2 values of 55.52/56 d.o.f and 55.08/56 d.o.f respectively). The derived photon index is $\Gamma = 1.88 \pm 0.03$, which is consistent with that of other ultraluminous X-ray sources in nearby spiral galaxies (e.g., Makishima et al. 2000; Li et al. 2006). The absorption column density is determined with $N_{\text{H}} \sim 2 \times 10^{21} \text{ cm}^{-2}$, about four times that of the Galactic absorption. The measured 0.5–2 keV and 2–10 keV X-ray flux are $1.38 \times 10^{-13} \text{ erg cm}^{-2} \text{ s}^{-1}$ and $3.49 \times 10^{-13} \text{ erg cm}^{-2} \text{ s}^{-1}$ respectively. From the thermal bremsstrahlung model, the thermal temperature (kT) is $5.57 \pm 0.92 \text{ keV}$, which is comparable to that of other X-Ray Binaries (XRBs) (e.g., Irwin et al. 2003).

However, the MCD model gives a poorer description of the data than the first two models (χ^2 : 62.94/56 d.o.f). We then add an additional component to the MCD model, a power law component (a multicolor blackbody component plus a power law component, the typical model for the black hole X-ray binaries, BH-XRBs) and a blackbody component (a multicolor blackbody component plus a second blackbody component, the typical model for neutron star X-ray binaries, NS-XRBs, e.g., Tanaka 2000). Both models lead to a significant improvement in the goodness of fit with acceptable

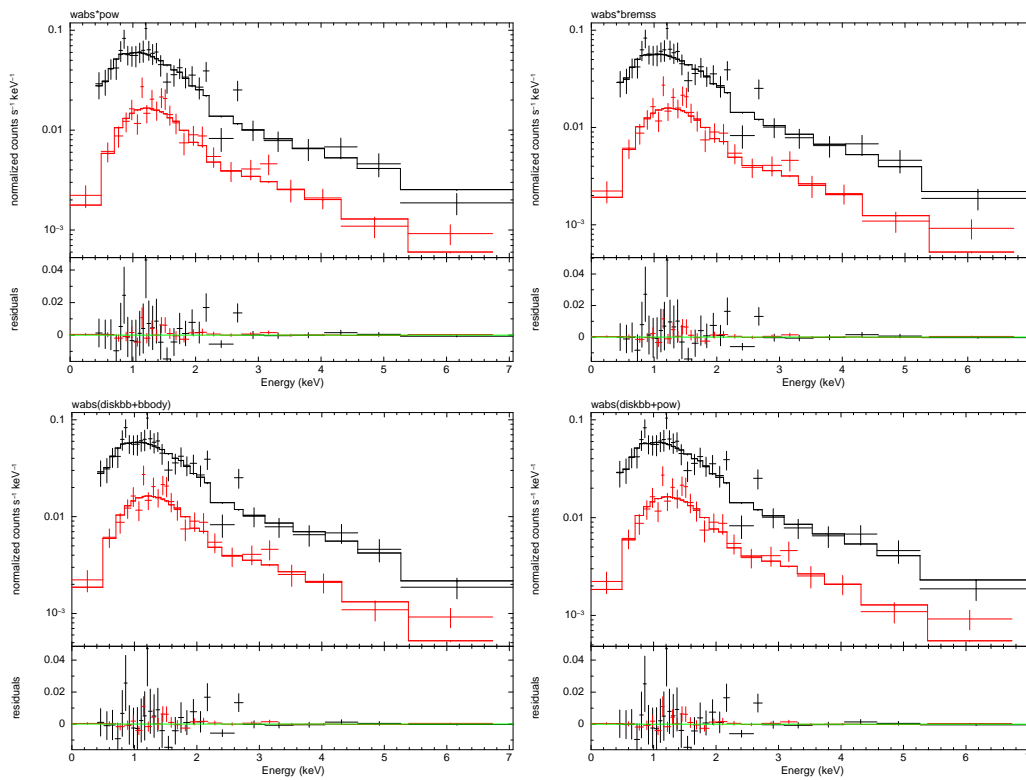


Fig. 5 XMM-Newton spectra of the prominent bright source 2XMMJ230457.6+122028 and four alternative fitting models: the power law model (wabs*pow in XSPEC, *upper left*), the thermal bremsstrahlung model (wabs*bremss, *upper right*), the multicolor blackbody disk plus blackbody model (wabs*(diskbb+body), *lower left*), the multicolor blackbody disk plus power-law model (wabs*(diskbb+pow), *lower right*). *Black*: PN spectrum, *red*: MOS spectrum (see electronic version).

parameters ($\chi^2=54.45/56$ d.o.f and $54.66/56$ d.o.f. respectively). The resulting temperatures of the innermost disk (kT_{in}) are 0.59 ± 0.17 keV and 1.86 ± 1.68 keV respectively from these two models, which show the existence of a high temperature disk, in accordance with the typical values of ultra-luminous X-ray sources in nearby spiral galaxies (e.g., Makishima et al 2000). The spectra with all four alternative models and residuals are shown in Figure 5 and detailed fitting results are presented in Table 3.

4 DISCUSSION

4.1 Nuclear X-ray Source

Is this object's nuclear emission related to star formation or AGN activity? Based on its large and centrally concentrated $10\text{-}\mu\text{m}$ flux, the nucleus has been classified as a starburst (Devereux 1989). However, based on its optical emission line spectra, it is very likely to be an active galactic nucleus, LINER (Keel 1983) or Seyfert 1.9 (Ho et al. 1997). Its VLA continuum observations show the existence of an anomalous 15-kpc scale ‘‘S’’ shaped double-jet with the north side being stronger than the south side, which is most likely driven by the active nucleus of the galaxy (Laine & Beck 2008). Its

Table 3 Spectral Fitting Results of the Brightest X-ray Source 2XMM J230457.6+122028

Model	N_{H}^a (10^{22} cm^{-2})	Γ^b	kT^c (keV)	kT_{in}^d (keV)	kT^e (keV)	Flux _{obs} ^f	Flux _{int.} ^g	$\chi^2/\text{d.o.f}$
I	0.25±0.03	1.88±0.03	—	—	—	~3.49	~3.57	55.52/56
II	0.18±0.02	—	5.57±0.92	—	—	~3.20	~3.28	55.08/56
III	0.07±0.03	—	—	1.39±0.09	—	~2.85	~2.87	62.94/56
IV	0.15±0.08	—	—	0.59±0.17	1.25±0.25	~3.02	~3.07	54.45/56
V	0.25±0.14	2.11±1.51	—	1.86±1.68	—	~3.26	~3.35	54.66/56

Model I: single absorbed power law (wabs*pow in XSPEC), Model II: absorbed thermal bremsstrahlung (wabs*bremss), Model III: the multicolor blackbody disk model (wabs*diskbb), Model IV: the multicolor blackbody disk plus blackbody model (wabs*(diskbb+bbbody)), Model V: the multicolor blackbody disk plus power-law model (wabs*(diskbb+pow)).

^a X-ray line-of-sight absorbing column density.

^b The photon index.

^c The temperature of thermal plasma.

^d The color temperature at the innermost disk radius.

^e The blackbody temperature.

^f Observed flux at 2–10 keV, in units of $10^{-13} \text{ erg cm}^{-2} \text{ s}^{-1}$.

^g Unabsorbed flux at 2–10 keV, in units of $10^{-13} \text{ erg cm}^{-2} \text{ s}^{-1}$.

XMM-Newton observations are analyzed here and its extended X-ray emissions tend to follow the orientation of its northern jet, which may be a sign of interaction between its nuclear jet and circum-nuclear gas. The 2–10 keV absorption-corrected flux is $1.3 \times 10^{-12} \text{ erg cm}^{-2} \text{ s}^{-1}$, corresponding to its intrinsic luminosity of $1.8 \times 10^{41} \text{ erg s}^{-1}$. Modeling the spectra obviously shows the presence of a strong iron fluorescent line (EW $\sim 1.5 \text{ keV}$ from our best-fitting model) and high density absorption ($N_{\text{H}} \sim 6.9 \times 10^{23} \text{ cm}^{-2}$) toward the nuclear region. In addition, the H₂O maser emission line around the systemic recession velocity of the galaxy is detected in its nuclear region. The maser isotropic luminosity of $19 L_{\odot}$ suggests that the maser should be associated with an AGN (e.g., Henkel et al. 2005). Moreover, a number of high-velocity maser components were also detected, which possibly implies the maser emission is from an edge-on nuclear accretion disk (Braatz & Gugliucci 2008). In summary, all these suggest the existence of one heavily obscured AGN.

4.2 The Nature of 2XMM J230457.6+122028?

The projected position of the brightest X-ray source is at the tip of the northern arm, through comparing its optical and XMM-Newton images. Is this prominent X-ray source intrinsic to NGC 7479? The spiral galaxy lies at a galactic latitude of -42° and the Galactic absorption column density is $\sim 5.29 \times 10^{20} \text{ cm}^{-2}$. Our spectral fitting results of the brightest X-ray source clearly show additional absorption over the Galactic column density (the derived column density of $\sim 2 \times 10^{21} \text{ cm}^{-2}$, ~ 4 times the Galactic column density). So the possibility of it being a foreground Galactic source could be excluded. In addition, the brightest source is located $\sim 80''$ away from the nucleus of NGC 7479 ($\sim 12 \text{ kpc}$) and the possibility of finding another AGN within such a small separation angle can basically be excluded from the Deep ROSAT All-sky Survey (Reynolds et al. 1997). From the relation of $\log N - \log S$ (Moreti et al. 2003), the number density of AGNs from our measured flux is $\sim 0.1 \text{ deg}^{-2}$. Thus, the probability of the existence of a background AGN can be estimated to be less than 10^{-4} . So, we propose that the brightest X-ray source should belong to the spiral galaxy NGC 7479.

Most of the brightest X-ray sources in the spiral arm are X-ray binaries (e.g., Luo et al. 2007). For 2XMM J230457.6+122028, its 0.5–10 keV unabsorbed luminosity is $8.2 \times 10^{40} \text{ erg s}^{-1}$ (for

the 20'' region) and 3.6×10^{40} erg s⁻¹ (for the 6'' region), based on its measured flux (from the power law model) and the stated redshift $z = 0.007942$ of NGC 7479. This result is consistent with that of ultra-luminous X-ray sources detected in the Cartwheel galaxy (Gao et al. 2003), but bigger than that of the most luminous ones in the Antennae galaxies (Miller et al. 2004). Such high luminosity requires a compact object with several hundred solar masses, within the Eddington limit of the accretion rate. The extreme high mass value of this accreting compact object excludes the possibility of it being an NS-XRB (mass limit of $\sim 3 M_{\odot}$), although the measured innermost disk temperature kT_{in} of ~ 1.8 keV is consistent with NS-XRB features (e.g., Tanaka 2000). Because of its very high luminosity, this kind of X-ray source has been suggested to have Eddington or sub-Eddington accretion onto one type of an accreting BH with masses intermediate between stellar mass ($\leq 20 M_{\odot}$) and active galactic nuclei ($10^6 M_{\odot} \sim 10^9 M_{\odot}$) (e.g., Reynolds et al. 1997). In addition, anisotropically-emitting BH-XRBs are also presumed to explain such kind of non-nuclear ultraluminous phenomenon. The X-ray emission is highly collimated toward us and the apparent X-ray luminosity is much higher than its intrinsic luminosity (Swartz et al. 2004). Further observations are really needed to probe the nature of 2XMM J230457.6+122028, e.g., Chandra observations with high spatial resolution; the optical spectroscopy data for its radial velocity; searching for possible X-ray variability, etc.

4.3 Constraints on Maser Disk Parameters

The maser spectra of NGC 7479 include a narrow red-shifted 140 mJy line at 2532 km s⁻¹ and some weaker high velocity components. Assuming the lines originate in an edge-on nuclear disk, the implied rotation speeds range up to 280 km s⁻¹ from the systemic velocity of 2381 km s⁻¹ (Braatz & Gugliucci 2008). Using the empirical relation $\log(M_{\text{BH}}/M_{\odot}) = \alpha + \beta \log(\sigma/\sigma_0)$ (Tremaine et al. 2002, $\alpha = 8.13$, $\beta = 4.02$, $\sigma_0 = 200$ km s⁻¹, and the velocity dispersion of $\sigma = 109$ km s⁻¹, taken from McElroy 1995), we can estimate the mass of its central engine $M_{\text{BH}} = 1.18 \times 10^7 M_{\odot}$. Then, we can constrain the radius of the molecular maser disk to be ~ 0.7 pc from the assumed rotation velocity $V = 280$ km s⁻¹ and the estimated BH mass, assuming Keplerian rotation of the maser disk. The results are consistent with those of some other possible disk-maser galaxies, NGC 1068, NGC 3079, Mrk 1210, etc., which were classified as Group B disk-masers from a geometrically thick structure with flattened rotation curves (Tilak et al. 2008; Zhang & Fan 2009). In addition, the dimensionless accretion rate ($L_{\text{bol}}/L_{\text{Edd}}$) can also be estimated, which is one of the most important parameters of the accretion disk. We use the ratio of $L_{2-10\text{keV}}/L_{\text{Edd}}$ as an estimate of the accretion rate, since $L_{2-10\text{keV}}$ is proportional to L_{bol} assuming a constant bolometric correction (Winter et al. 2009). The Eddington luminosity L_{Edd} is estimated to be $L_{\text{Edd}} = 1.53 \times 10^{45}$ erg s⁻¹ from the value $1.3 \times 10^{46} (M/10^8 M_{\odot})$ erg s⁻¹. Then we get the estimated accretion rate $\log(L_{2-10\text{keV}}/L_{\text{Edd}})$ of -3.9 , which is consistent with that of the archetypal disk maser NGC 4258 (Guo et al. 2009).

5 CONCLUSIONS

In this paper, we present the *XMM-Newton* observations of NGC 7479. The main results are summarized as follows:

- (1) Its smoothed image clearly shows X-ray spiral morphology, which is consistent with its optical asymmetric spiral structure. Relative to the weak nucleus, one bright X-ray source (2XMM J230457.6+122028, $\sim 50\%$ higher count rate) can be found at the tip of the northern arm. Both the nuclear source and the prominent source showed no significant variations during the exposure time.
- (2) For the nuclear X-ray source, the hard X-ray spectra are best fit by a partial absorbed power model with high absorbing column density of $N_{\text{H}} \sim 6.9 \times 10^{23}$ cm⁻². The notable iron fluorescent

line (EW of ~ 1.5 keV) and detected nuclear H₂O maser spots (possibly with a disk maser origin) support the existence of a heavily obscured AGN-like nucleus.

- (3) For the brightest X-ray source, its spectra can be best described by an absorbed power law with a column density of $\sim 2.5 \times 10^{21}$ cm⁻², about four times the Galactic column density. It should be intrinsic to NGC 7479 and its 0.5–10 keV unabsorbed luminosity is 8.2×10^{40} erg s⁻¹. Our analysis suggests that it might be a BH-XRB (medium mass BH with several hundred solar masses or an anisotropically-emitting BH). However, more observations and analyses are needed to further probe its nature.
- (4) Maser disk parameters are constrained from its maser spectra and our estimated BH mass of $1.18 \times 10^7 M_{\odot}$. The rotation velocity of the maser disk, the disk radius and the accretion rate ($L_{2-10 \text{ keV}}^{\text{ac}}/L_{\text{Edd}}$) are determined to be ~ 280 km s⁻¹, ~ 0.7 pc and 1.2×10^{-4} respectively.

Acknowledgements We are grateful to the anonymous referee for his/her constructive comments, which greatly improved the quality of the manuscript. We also thank Dr. Z.Y. Li for his help on data analysis and his many helpful comments. This work is partly supported by the National Natural Science Foundation of China (Grant No. 10633010) and the Guangdong provincial Natural Science Foundation (8451009101001047). It is based on observations obtained with XMM-Newton, an ESA science mission with instruments and contributions directly funded by ESA member states and the USA (NASA). We made use of the NASA Astrophysics Data System Bibliographic Services (ADS) and also the NASA/IPAC Extragalactic Database (NED), which is operated by the Jet Propulsion Laboratory.

References

- Braatz, J. A., Wilson, A. S., & Henkel, C. 1997, ApJS, 110, 321
- Braatz, J. A., & Gugliucci, N. E. 2008, ApJ, 678, 96
- Braatz, J. A. 2009, astro2010: The Astronomy and Astrophysics Decadal Survey, 2010, 23
- Devereux, N. A. 1989, ApJ, 346, 126
- Gao, Y., Wang, Q. D., Appleton, P. N., & Lucas, R. A. 2003, ApJ, 596, L171
- Greenhill, L. J., Tilak, A., & Madejski, G. 2008, ApJ, 686, L13
- Guo, Q., Zhang, J. S., & Fan, J. H. 2009, IJMPD, 1809, 1367
- Henkel, C., Peck, A. B., Tarchi, A., et al. 2005, A&A, 436, 75
- Ho, L. C., Filippenko, A. V., & Sargent, W. L. W. 1997, ApJS, 112, 315
- Irwin, J. A., Athey, A. E., & Bregman, J. N. 2003, ApJ, 587, 356
- Kajava, J. J. E., & Poutanen, J. 2009, MNRAS, 398, 1450
- Kalberla, P. M. W., Burton, W. B., & Hartmann, D., et al. 2005, A&A, 440, 775
- Keel, W. C. 1983, ApJS, 52, 229
- Kondratko, P. T., Greenhill, L. J., & Moran, J. M. 2006, ApJ, 652, 136
- Laine, S., & Heller, C. H. 1999, MNRAS, 308, 557
- Laine, S., & Beck, R. 2008, ApJ, 673, 128
- Li, Z., Wang, Q. D., Irwin, J. A., et al. 2006, MNRAS, 371, 147
- Luo, B., Chen, J.-Y., Zhang, Z.-L., Wang, Y., Wang, J.-Y., & Xu, H.-G. 2007, ChJAA (Chin. J. Astron. Astrophys.), 7, 335
- Madejski, G., Done, C., Zycki, P. T., & Greenhill, L. 2006, ApJ, 636, 75
- Makishima, K., Kubota, A., Mizuno, T., et al. 2000, ApJ, 535, 632
- McElroy, D. B. 1995, ApJS, 100, 105
- Mewe, R., Gronenschild, E. H. B. M., & van den Oord, G. H. J. 1985, A&AS, 62, 197
- Miller, J. M., Zezas, A., Fabbiano, G., & Schweizer, F. 2004, ApJ, 609, 728
- Moran, E. C., Kay, L. E., Davis, M., et al. 2001, ApJ, 556, L75

- Moretti, A., Campana, S., Lazzati, D., & Tagliaferri, G. 2003, *ApJ*, 588, 696
- Quillen, A., Frogel, J. A., Kenney, J. D. P., et al. 1995, *ApJ*, 441, 549
- Reynolds, C. S., Loan, A. J., Fabian, A. C., et al. 1997, *MNRAS*, 286, 349
- Su, J.-B., Zhang, J.-S., & Fan, J.-H. 2008, *ChJAA* (Chin. J. Astron. Astrophys.), 8, 547
- Swartz, D. A., Ghosh, K. K., Tennant, A. F., & Wu, K. 2004, *ApJS*, 154, 519
- Tanaka, Y. 2000, *IAUS*, 195, 37
- Tilak, A., Greenhill, L. J., Done, C., & Madejski, G. 2008, *ApJ*, 678, 701
- Tremaine, S., Gebhardt, K., Bender, R., et al. 2002, *ApJ*, 574, 740
- Tully, R. B. 1988, *Nearby Galaxies Catalog* (Cambridge: Cambridge Univ. Press)
- Winter, L. M., Mushotzky, R., Reynolds, C. S., & Tueller, J. 2009, *ApJ*, 690, 1322
- Zhang, J. S., Henkel, C., Kadler, M., et al. 2006, *A&A*, 450, 933
- Zhang, J. S., & Fan, J. H. 2009, *Science in China G: Physics and Astronomy*, 52, 960
- Zhang, J. S., Henkel, C., Guo, Q., et al. 2010, *ApJ*, 708, 1528